Magnetic and Mössbauer spectral study of $ErFe_{11}Ti$ and $ErFe_{11}TiH$

Cristina Piquer, Raphaël P. Hermann, and Fernande Grandjean[a)]
Department of Physics, B5, University of Liège, B-4000 Sart-Tilman, Belgium

Gary J. Long[b)]
Department of Chemistry, University of Missouri-Rolla, Rolla, Missouri 65409-0010

Olivier Isnard[c)]
Laboratoire de Cristallographie, CNRS, associé à l'Université J. Fourier, BP 166X, F-38042 Grenoble Cedex, France

(Received 19 September 2002; accepted 14 December 2002)

X-ray diffraction, isothermal magnetization at 5 and 300 K, ac magnetic susceptibility measurements between 5 and 200 K, and iron-57 Mössbauer spectral measurements between 4.2 and 295 K have been carried out on $ErFe_{11}Ti$ and $ErFe_{11}TiH$. Hydrogen uptake has been measured by gravimetric analysis and the insertion of hydrogen into $ErFe_{11}Ti$ increases its magnetization, magnetic hyperfine fields, and isomer shifts as a result of the associated lattice expansion. Peaks and steplike changes in both the real and imaginary components of the ac magnetic susceptibility are observed at ~ 50 and 40 K for $ErFe_{11}Ti$ and $ErFe_{11}TiH$, respectively, and are assigned to spin-reorientation transitions resulting from the temperature dependence of the sixth-order Stevens crystal-field term of erbium. The Mössbauer spectra have been analyzed with a model which considers both these spin reorientations and the distribution of titanium atoms in the near-neighbor environment of the three crystallographically distinct iron sites. The assignment and the temperature dependencies of the hyperfine fields and isomer shifts are in complete agreement with the Wigner–Seitz cell analysis of the three iron sites in $ErFe_{11}Ti$ and $ErFe_{11}TiH$. The changes in the hyperfine field and isomer shift with the number of titanium near neighbors of the three iron sites are in agreement with the values observed for related titanium–iron intermetallic compounds. © *2003 American Institute of Physics.* [DOI: 10.1063/1.1544087]

I. INTRODUCTION

Modern high performance magnets are based on $3d-4f$ intermetallic compounds in which the $3d$ element, usually Fe or Co, is the major component and is responsible for the high remanence and Curie temperature, and the $4f$ element, usually a light rare-earth such as Nd or Sm, provides some additional magnetization and, most important, a high magnetic anisotropy. The appropriate combination of these elements can lead to both a high magnetization and coercivity and thus a strong magnet. Among the possible iron-rich materials, the $RFe_{12-x}M_x$ compounds, where R is a rare-earth and M is Ti, V, Cr, Nb, Mo, Ta, or W, with the I4/mmm $ThMn_{12}$ structure,[1–4] are promising for their applications as permanent magnet materials. This series of intermetallic compounds offers two main advantages as hard magnetic materials; first, a high iron content which yields a high magnetization and, second, a relatively high Curie temperature, especially for the titanium containing compounds. Hence, a good deal of attention has been devoted to these tetragonal compounds[5–7] and, because of its excellent properties, $SmFe_{11}Ti$ has been identified as potentially the most promising compound.[8–10]

In general, the insertion of light elements, such as hydrogen, carbon, or nitrogen, into the structure of a rare-earth transition metal intermetallic compound has a dramatic and beneficial effect upon the compound's magnetic properties.[11] Indeed, the insertion of interstitial elements into the $RFe_{11}Ti$ compounds leads to large changes in their structural and magnetic properties.[8,9,12–15]

$ErFe_{11}Ti$, as well as several other $RFe_{11}Ti$ compounds,[16–18] exhibit a spin reorientation at low temperature, a spin reorientation which has been extensively studied.[10,19–23] The influence of interstitial hydrogen on the magnetocrystalline anisotropy of $ErFe_{11}Ti$ has also been reported[21] earlier.

Herein, we investigate the influence of the insertion of hydrogen into the crystal lattice of $ErFe_{11}Ti$ upon its spin reorientation and, more specifically, the iron sublattices by combining macroscopic isothermal magnetization and ac susceptibility measurements with microscopic iron-57 Mössbauer spectral measurements.

II. EXPERIMENT

$ErFe_{11}Ti$ has been synthesized in a water cooled copper crucible by melting 99.95% pure elements in a high-frequency induction furnace. A high homogeneity was achieved by annealing the sample at 1200 K for 10 days. The hydrogen insertion was carried out under 20 bar of H_2 gas

a)Electronic mail: fgrandjean@ulg.ac.be
b)Electronic mail: glong@umr.edu
c)Electronic mail: isnard@grenoble.cnrs.fr

TABLE I. The lattice parameters, Curie temperatures, and saturation magnetizations of $ErFe_{11}Ti$ and $ErFe_{11}TiH$

Compound	a (Å)	c (Å)	c/a	V (Å^3)	T_C (K)	$M_s^{5\ K}$ (μ_B/f.u.)	$M_s^{300\ K}$ (μ_B/f.u.)
$ErFe_{11}Ti$	8.481(1)	4.783(1)	0.56391	344.1	518(4)	9.8	14
$ErFe_{11}TiH$	8.519(1)	4.791(1)	0.56233	347.6	574(6)	10.6	15

after a short thermal activation was used to initiate the insertion. The hydrogen content was determined by the gravimetric mass-gain method.

X-ray diffraction patterns were recorded with a Guinier–Hägg focusing camera and 1.9373 Å Fe $K\alpha_1$ radiation; silicon powder was used as an internal standard. The lattice parameters have been refined from 24 observed Bragg reflections.

The thermomagnetic analyses of the samples, sealed in a silica tube under hydrogen gas to avoid oxidation and hydrogen loss, were performed on a Faraday balance. The isothermal magnetization curves were obtained at 5 and 300 K with the extraction method[24] in a dc field of up to 7 T. The saturation magnetization values have been derived, as discussed[24] earlier by extrapolation to zero field of the magnetization results obtained in fields above 4 T. The low-temperature ac magnetic susceptibilities were obtained on a computer controlled mutual inductance susceptometer[25] at an exciting field of 10^{-4} T and a frequency of 120 Hz. A lock-in amplifier was used to measure the complex susceptibility, $\chi_{ac}=\chi'-j\chi''$, where χ' is the initial susceptibility, a quantity which is related to the variation in the sample magnetization, and χ'' is nonzero if magnetic energy is absorbed by the sample. The temperature dependence of the real component, χ', and the imaginary component, χ'' of the ac susceptibility were measured in order to determine the temperatures of the magnetic phase transitions. These measurements are very sensitive to the onset of the magnetic phase transition caused by changes in the anisotropy energy. The real part of the ac susceptibility is determined predominately by the changes in both the magnetic anisotropy energy and the domain-wall energy, whereas the imaginary ac susceptibility reflects energy absorption by the sample, an energy which is mainly derived from domain-wall movement.

The Mössbauer spectra were measured between 4.2 and 295 K on a constant-acceleration spectrometer which utilized a rhodium matrix cobalt-57 source and was calibrated at room temperature with α-iron foil. The Mössbauer spectral absorbers contained 35 mg/cm^2 of powdered sample which had been sieved to a 0.045 mm or smaller diameter particle size. The low-temperature spectra were obtained in a Janis Super-varitemp cryostat and the temperature was controlled with a Lakeshore Cryogenics temperature controller with an accuracy of better than 1% of the observed temperature. The resulting spectra have been fit as discussed next and the estimated errors are at most $\pm$ 0.2 T for the hyperfine fields and their changes upon hydrogenation, $\pm$ 0.01 mm/s for the isomer shifts and their changes, and $\pm$ 0.02 mm/s for the quadrupole shifts and their changes. The observed linewidths were typically 0.38 ± 0.02 mm/s.

III. STRUCTURAL AND MAGNETIC RESULTS

$ErFe_{11}Ti$ crystallizes in the $ThMn_{12}$ tetragonal structure with space group I4/mmm. In this structure, the iron atoms occupy three inequivalent crystallographic sites, the 8*f*, 8*i*, and 8*j* sites, and the erbium occupies the 2*a* site. The titanium atoms are found[12,26,27] only on the 8*i* site, the largest of the three iron sites. Neutron diffraction investigations[12,27] indicate that the hydrogen is inserted into the 2*b* site, an octahedral site with two erbium and four 8*j* near neighbors. Consequently, the maximum hydrogen uptake per formula unit is one. Gravimetric analysis of $ErFe_{11}TiH$ indicates that the maximum hydrogen uptake has been achieved and that there is one hydrogen atom per formula unit.

The lattice parameters and the unit-cell volume of $ErFe_{11}Ti$ and $ErFe_{11}TiH$ are given in Table I. Hydrogen insertion induces a significant increase of 3.5 Å^3 or one percent in the unit-cell volume. This increase is anisotropic and occurs mainly in the (a,b) basal plane. Both the lattice parameters and their increase upon hydrogenation are significantly larger than previously reported.[23] This larger increase probably indicates that the hydrogen uptake in the $ErFe_{11}TiH$ sample studied earlier was less than in the sample studied herein.

The insertion of hydrogen into $ErFe_{11}Ti$ to form $ErFe_{11}TiH$ produces a significant increase in the Curie temperature from 518 to 574 K. In the earlier study,[23] a smaller increase from 515 to 563 K has been reported, a smaller increase which also indicates that the hydrogen uptake was less than one in the earlier study. Similar increases in Curie temperature have been reported[3,9,28–30] for several isotypic compounds. These increases are related to the increase in the iron–iron interatomic distances and the concomitant increase in the $3d-3d$ magnetic exchange interactions.

The isothermal magnetization curves shown in Fig. 1 reveal that the insertion of hydrogen into $ErFe_{11}Ti$ increases the 5 K saturation magnetization from 9.8 to 10.6 μ_B per formula unit, and the 300 K values from 14 to above 15 μ_B per formula unit. The saturation magnetization is larger at 300 K than at 5 K because the erbium contribution to the magnetization is opposed to the iron contribution and decreases rapidly with increasing temperature. Further, at 300 K $ErFe_{11}TiH$ exhibits a larger high-field susceptibility[21] than does $ErFe_{11}Ti$.

The spin-reorientation temperature was determined from the anomaly in the temperature dependence of the ac magnetic susceptibility, a technique which is known[18,31] to be very sensitive to changes in the magnetization direction in rare-earth transition-metal intermetallic compounds.

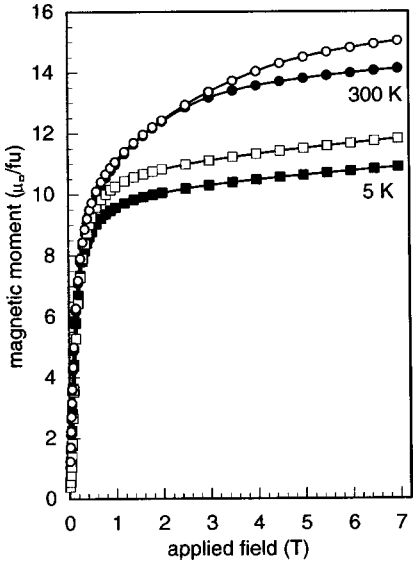

FIG. 1. The isothermal magnetization of $ErFe_{11}Ti$, closed symbols, and $ErFe_{11}TiH$, open symbols.

As is shown in Fig. 2 by the closed symbols, both the real and imaginary parts of the ac susceptibility of $ErFe_{11}Ti$ exhibit sharp peaks at 50 K, peaks which are undoubtedly assigned to the spin reorientation observed at this temperature. Indeed, in $ErFe_{11}Ti$, the easy magnetization direction is known[18] to change from parallel to the *c* axis above 50 K to canted from the *c* axis below 50 K. Because in the $RFe_{11}Ti$ structure, the iron sublattices favor a uniaxial magnetic anisotropy parallel to the *c* axis and erbium, like samarium, has a positive second-order Stevens coefficient, α_J, which reinforces the uniaxial magnetic anisotropy, $ErFe_{11}Ti$ would be expected to maintain this uniaxial anisotropy at all temperatures. However, the sixth-order crystal-field term is particularly important for erbium because of its large positive Stevens coefficient, γ_J. Hence, it is generally accepted[16–18,23,32] that the spin reorientation observed at 50 K in $ErFe_{11}Ti$ is due to the sixth-order term in the anisotropy energy, a term which gains importance as the temperature is lowered. In studies of $ErFe_{11}Ti$ single crystals,[16,23] the spin reorientation has been described as a transition from an alignment of the magnetic moments along the *c* axis above 50 K to a so-called ''easy-cone'' magnetic structure below 50 K. At temperatures below the spin-reorientation temperature, the magnetization tilts[16–18] progressively away from the *c* axis to reach a maximum tilt of $\sim 20°$.

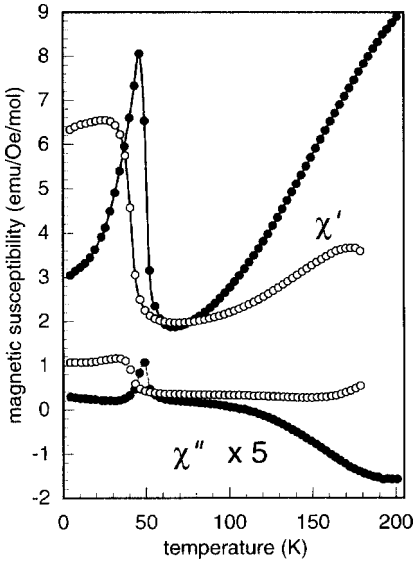

FIG. 2. The temperature dependence of the ac magnetic susceptibility for $ErFe_{11}Ti$, closed symbols, and $ErFe_{11}TiH$, open symbols.

Both the real and imaginary portions of the ac susceptibility of $ErFe_{11}TiH$ exhibit steplike changes at ~ 40 K as is shown in Fig. 2 by the open symbols. A peak at 41 K has also been observed[23] in the remanent magnetization of $ErFe_{11}TiH$ and assigned to a spin reorientation similar to that observed for $ErFe_{11}Ti$. However, the completely different temperature dependencies of the ac susceptibility for $ErFe_{11}Ti$ and $ErFe_{11}TiH$ may indicate that the spin reorientations may be of a different nature. The persistence of the spin reorientation in $ErFe_{11}TiH$ at only a slightly smaller temperature than in $ErFe_{11}Ti$, indicates that the interstitial hydrogen atoms do not drastically modify the electric-field gradient at the erbium site. However, it is difficult to predict the influence of the inserted hydrogen on the anisotropy parameters, particularly the higher-order crystal-field terms, of the erbium sublattice anisotropy.

In the isotypic $GdFe_{11}Ti$ and $GdFe_{11}TiH$ compounds, Isnard *et al.*[28] have shown by gadolinium-155 Mössbauer spectroscopy that hydrogen insertion increases the electric-field gradient at the gadolinium site and enhances the second-order contribution of the gadolinium sublattice to the magnetocrystalline anisotropy. Because there are no experimental results on the influence of hydrogen insertion on the crystal field terms above the second order, to our knowledge, it is difficult to predict the evolution of the $ErFe_{11}Ti$ magnetic phase diagram versus hydrogen content. In order to investigate the effect of the hydrogen insertion on the iron sublattices, we have carried out an iron-57 Mössbauer spectral study of $ErFe_{11}Ti$ and $ErFe_{11}TiH$ between 4.2 and 295 K.

IV. MÖSSBAUER SPECTRAL MEASUREMENTS

The Mössbauer spectra of $ErFe_{11}Ti$ and $ErFe_{11}TiH$ obtained between 4.2 and 295 K are shown in Figs. 3 and 4, respectively. Because iron atoms occupy the three inequivalent 8*f*, 8*i*, and 8*j* crystallographic sites and the titanium atoms occupy only the 8*i* sites, at least three sextets assigned to the 8*f*, 8*i*, and 8*j* sites, with relative areas in the ratio of 8:6:8 are required to fit the spectra. However, as already noted[3] in our study of $CeFe_{11}Ti$ and $CeFe_{11}TiH$, these three sextets must be further subdivided to take into account the distribution of the titanium atoms in the neighborhood of the three iron sites.

The random occupation of the the 8*i* sites by the titanium atoms results in a binomial distribution of the titanium near neighbors of the three iron sites. Hence, the 8*i* sextet is subdivided into three sextets with 6.47, 10.79, and 9.98 percent areas, and each of the 8*f* and 8*j* sextets is subdivided into three sextets with 11.51, 15.34, and 9.52 percent areas, sextets which represent the iron with zero, one, and two or more

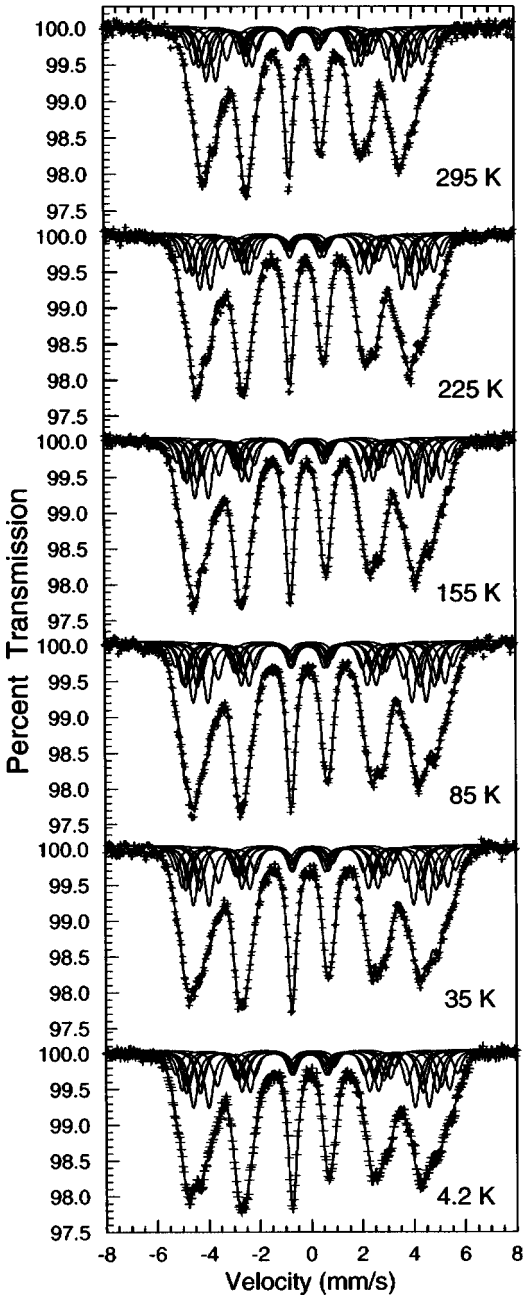

FIG. 3. The Mössbauer spectra of $ErFe_{11}Ti$ obtained at the indicated temperatures.

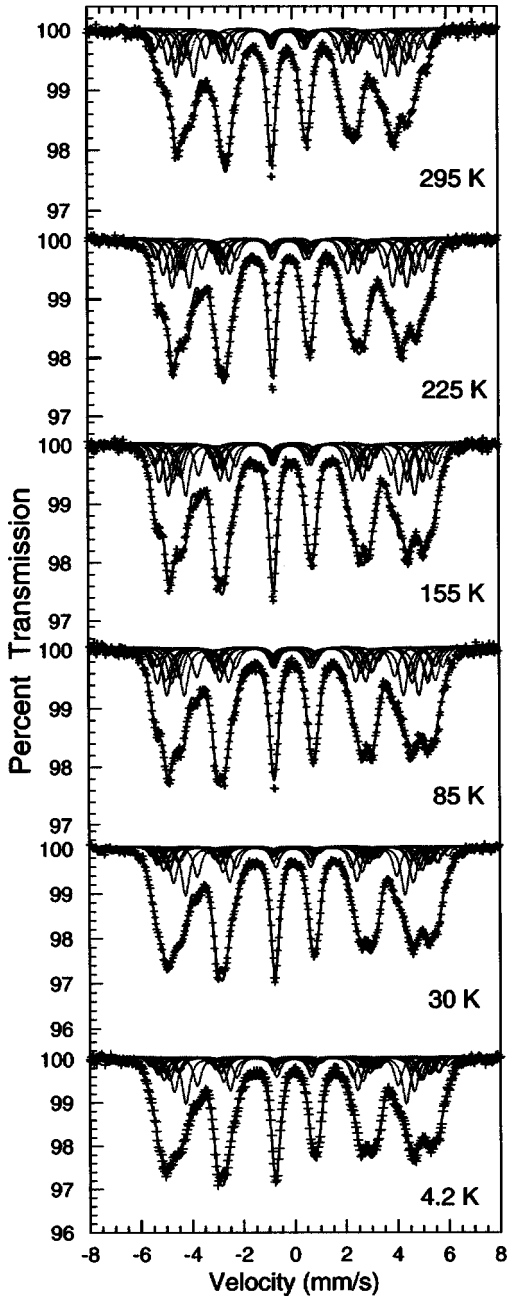

FIG. 4. The Mössbauer spectra of $ErFe_{11}TiH$ obtained at the indicated temperatures.

titanium near neighbors, respectively. Hence, at least nine sextets, with their areas fixed to the aforementioned relative values, are required to accurately model the Mössbauer spectra of $ErFe_{11}Ti$ and $ErFe_{11}TiH$ above their spin-reorientation temperatures in the uniaxial magnetic phase. Below the spin-reorientation temperatures in the conical magnetic phase, even more sextets are required (see next). It should be noted that the presence of 5% percent of α-iron has been observed in the spectra of $ErFe_{11}TiH$ and has been fit with a sextet with hyperfine parameters constrained to the known hyperfine parameters of α-iron.

Three hyperfine parameters define each sextet, the hyperfine field, H, the isomer shift, δ, and the quadrupole shift, ε. In order to both build in constraints into the model and reduce the number of adjustable parameters, we assume that the three hyperfine parameters for each crystallographically inequivalent iron site vary linearly with the number, n, of titanium near neighbors, as given by

$$H_n = H_0 + n\Delta H,$$
$$\delta_n = \delta_0 + n\Delta\delta,$$

and

$$\varepsilon_n = \varepsilon_0 + n\Delta\varepsilon,$$

where H_0, δ_0, and ε_0 are the hyperfine field, isomer shift, and quadrupole shift, respectively, for zero titanium near neighbor and ΔH, $\Delta\delta$, and $\Delta\varepsilon$, are the changes in the hyperfine field, isomer shift, and quadrupole shift, respectively,

TABLE II. Mössbauer hyperfine parameters for $ErFe_{11}Ti$

Parameter	T (K)	$8i$	$8j$	$8f$	Wt. average
H_0 (ΔH) (kOe)	4.2	341 (−17)	321 (−18)	270 (−20)	283
	30	339 (−17)	303 (−19)	269 (−23)	280
	70	336 (−18)	301 (−19)	270 (−23)	279
	85	336 (−18)	301 (−20)	270 (−23)	279
	155	329 (−18)	294 (−20)	264 (−23)	273
	225	316 (−17)	279 (−18)	254 (−23)	261
	295	293 (−17)	257 (−17)	236 (−22)	241
δ_0 ($\Delta\delta$) (mm/s)	4.2	0.150 (−0.024)	0.007 (−0.027)	−0.013 (0.002)	0.023
	30	0.143 (−0.028)	0.011 (−0.020)	−0.036 (0.024)	0.023
	70	0.115 (−0.010)	0.010 (−0.022)	−0.055 (0.035)	0.016
	85	0.111 (−0.015)	0.001 (−0.022)	−0.059 (0.030)	0.007
	155	0.101 (−0.030)	−0.022 (−0.019)	−0.101 (0.040)	−0.019
	225	0.045 (−0.027)	−0.052 (−0.026)	−0.149 (0.045)	−0.063
	295	−0.011 (−0.025)	−0.102 (−0.028)	−0.194 (0.044)	−0.113
ε_0 ($\Delta\varepsilon$) (mm/s)	4.2	0.118 (−0.021)	0.024 (0.015)	0.069 (0.011)	0.068
	30	0.106 (0.008)	0.006 (0.028)	0.063 (0.018)	0.072
	70	0.122 (0.012)	0.008 (0.027)	0.022 (0.030)	0.067
	85	0.128 (0.012)	0.009 (0.024)	0.035 (0.030)	0.073
	155	0.121 (0.011)	−0.006 (0.038)	0.019 (0.045)	0.069
	225	0.114 (0.001)	−0.023 (0.076)	−0.047 (0.075)	0.058
	295	0.091 (0.001)	−0.026 (0.085)	−0.044 (0.080)	0.056

for one additional titanium near neighbor. A similar linear dependence of the hyperfine field on the number of substitutional near-neighbor atoms has been successfully used[33–36] in the analysis of the Mössbauer spectra of the $R_2Fe_{17-x}M_x$ solid solutions. Hence, above the spin-reorientation temperature, the Mössbauer spectra of $ErFe_{11}Ti$ and $ErFe_{11}TiH$ are fit with nine sextets, which involve 18 hyperfine parameters, one linewidth, and one total absorption area. A similar model has been used[37] to fit the Mössbauer spectra of $YFe_{11}Ti$ and $YFe_{11}TiH$ at 20 and 295 K. As is shown in Figs. 3 and 4, all the fits above the spin-reorientation temperature of 50 K are very good and their hyperfine parameters are given in Tables II and III.

Below the spin-reorientation temperature, a further subdivision of the three sextets assigned to each inequivalent iron site may be necessary. Because of the canting of the iron magnetic moments and, consequently, of the hyperfine fields away from the *c* axis, multiple relative orientations of the principal axis of the electric-field gradient and of the hyperfine field occur and yield different angles, θ, between these two directions and hence different quadrupole shifts. A close examination of the symmetry at the three iron sites indicates that, if the hyperfine field is tilted away from the *c* axis, there is no further subdivision of the sextets representing the $8f$ site, whereas there is a further subdivision of those representing the $8i$ and $8j$ sites. Each sextet assigned to the $8i$ and $8j$

TABLE III. Mössbauer hyperfine parameters for $ErFe_{11}TiH$

Parameter	T (K)	$8i_I$	$8i_{II}$	$8j_I$	$8j_{II}$	$8f$	Wt. average
H_0 (ΔH) (kOe)	4.2	358 (−27)	354 (−24)	326 (−22)	331 (−17)	291 (−24)	299
	30	357 (−27)	352 (−24)	324 (−21)	331 (−18)	290 (−24)	298
	60	352 (−26)	···	328 (−22)	···	292 (−26)	297
	85	352 (−26)	···	327 (−22)	···	291 (−26)	296
	155	344 (−25)	···	316 (−21)	···	284 (−25)	289
	255	329 (−24)	···	304 (−20)	···	272 (−25)	276
	295	311 (−23)	···	287 (−18)	···	256 (−24)	261
δ_0 ($\Delta\delta$) (mm/s)	4.2	0.103 (0.079)	···	−0.015 (−0.011)	···	−0.044 (0.049)	0.044
	30	0.102 (0.079)	···	−0.015 (−0.011)	···	−0.048 (0.049)	0.042
	60	0.085 (0.083)	···	−0.008 (−0.008)	···	−0.066 (0.048)	0.036
	85	0.086 (0.079)	···	−0.014 (−0.011)	···	−0.068 (0.049)	0.031
	155	0.053 (0.077)	···	−0.051 (−0.004)	···	−0.097 (0.051)	0.000
	225	−0.012 (0.085)	···	−0.095 (0)	···	−0.143 (0.053)	−0.045
	295	−0.076 (0.093)	···	−0.140 (−0.009)	···	−0.172 (0.048)	−0.092
ε_0 ($\Delta\varepsilon$) (mm/s)	4.2	0.209 (−0.043)	−0.076(0.236)	−0.018 (0.064)	0.046 (−0.075)	0.042 (0.033)	0.073
	30	0.254 (−0.036)	−0.080 (0.212)	0.011 (0.029)	0.040 (−0.016)	0.035 (0.040)	0.080
	60	0.123 (0.096)	···	−0.037 (0.038)	···	−0.002 (0.057)	0.082
	85	0.127 (0.098)	···	−0.036 (0.035)	···	0.007 (0.055)	0.085
	155	0.084 (0.121)	···	−0.051 (0.052)	···	−0.021 (0.082)	0.080
	225	0.070 (0.119)	···	−0.072 (0.042)	···	0.003 (0.076)	0.071
	295	0.041 (0.140)	···	−0.096 (0.047)	···	0.009 (0.073)	0.064

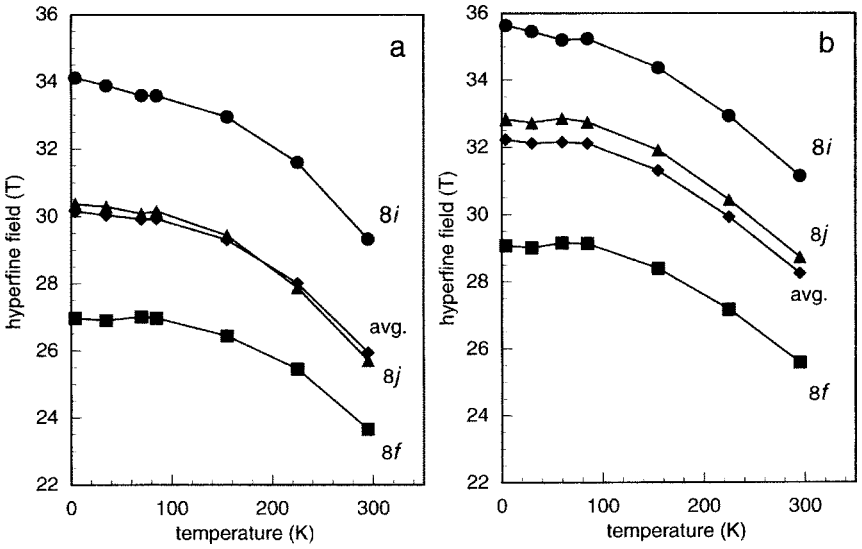

FIG. 5. The temperature dependence of the maximum hyperfine fields, H_0, at the three iron sites and their average in $ErFe_{11}Ti$ (a) and $ErFe_{11}TiH$ (b).

sites is subdivided into two sextets of equal relative areas with identical isomer shifts but different quadrupole shifts and slightly different hyperfine fields. This sextet subdivision is well established for the R_2Fe_{17} compounds, see for instance Ref. 39. Hence, below the spin-reorientation temperature, the Mössbauer spectra of $ErFe_{11}TiH$ are modeled with 15 sextets, which involve 26 hyperfine parameters, one linewidth, and one total absorption area. In contrast, in the case of $ErFe_{11}Ti$, for which the canting angle[18] of the moments from the *c* axis is small at only $\sim 20°$, the further subdivision of the 8*i* and 8*j* sextets was not necessary in order to obtain good fits below the spin reorientation. The fits below the spin reorientation, as may be seen in Figs. 3 and 4, are very good and their hyperfine parameters are also given in Tables II and III.

Because of the number of parameters just mentioned, it would seem that it should be easy to obtain good fits but that the fits may be far from unique. Hence, in Sec. V, we discuss the temperature dependencies of the hyperfine parameters and indicate how they give confidence to the spectral analysis, its physical meaning, and the extent of its uniqueness. Our experience indicates that it is not as easy as might be expected to find good fits of the observed spectra especially when physically viable changes in the hyperfine parameters with temperature are imposed upon the fits. Indeed, we have not been able to find an alternative model that both provided good fits and viable trends in the hyperfine parameters with temperature, but such an undiscovered model may, of course, exist.

V. DISCUSSION

A. Hyperfine fields

The assignment and temperature dependence of the three hyperfine fields for zero titanium near neighbor and their weighted average for $ErFe_{11}Ti$ and $ErFe_{11}TiH$ are shown in Figs. 5(a) and 5(b), respectively. A Wigner–Seitz cell analysis[38] of the three inequivalent iron sites in $ErFe_{11}Ti$ and $ErFe_{11}TiH$ indicates that the 8*i* site has at 11.75 the largest average number of iron near neighbors, whereas the 8*f* and 8*j* iron sites have only nine iron near neighbors. Consequently, the sextets with the largest hyperfine field, H_0, have been assigned to the 8*i* site, both on the basis of its percent contribution and its iron near-neighbor environment. As is indicated next, this assignment is further supported by the observed isomer shift values. Because of both their identical constrained percentage areas and iron near-neighbor environments, it is not possible to unequivocally assign the 8*f* and 8*j* sextets on the basis of their fields and their assignment is based on the isomer shift (see next). If the three H_0 hyperfine fields increase upon hydrogen insertion, the sequence of hyperfine fields, $8i > 8j > 8f$, remains unchanged as is shown in Fig. 5(b). Indeed, a Wigner–Seitz cell analysis[38] indicates that, in addition to the lattice expansion, hydrogen insertion adds only one hydrogen to the near-neighbor environment of the 8*j* site; the 8*f* and 8*i* sites do not have any hydrogen near neighbors.

The temperature dependence of the increase in the three hyperfine fields upon hydrogenation is shown in Fig. 6. The three hyperfine fields increase because of the lattice expansion and the 8*j* hyperfine field increases the most because of its added near-neighbor hydrogen. Similar increases in hyperfine field upon hydrogenation or nitrogenation of several R_2Fe_{17} compounds have been observed.[31,39,40] The larger increases observed at 295 K in Fig. 6 result because the Curie temperature of $ErFe_{11}Ti$ is closer to 295 K than is that of $ErFe_{11}TiH$.

The changes in the hyperfine field per titanium near neighbor are -2.5 ± 0.2 T for the 8*f* and 8*i* sites and -2.0 ± 0.2 T for the 8*j* site, where the errors reflect the variations in the difference with temperature between 4.2 and 295 K. Hence, we can conclude, as expected, that these changes are relatively independent of temperature below 295 K. The observed decreases in the hyperfine fields upon the replacement of one iron by one titanium near neighbor are very similar to those observed[3,37] in both $YFe_{11}Ti$ and $CeFe_{11}Ti$ and their hydrides and are within the range of -1.1 to -6 T observed in a spinel oxide[41] and in $Nd_2Fe_{16}Ti$, [42] respectively.

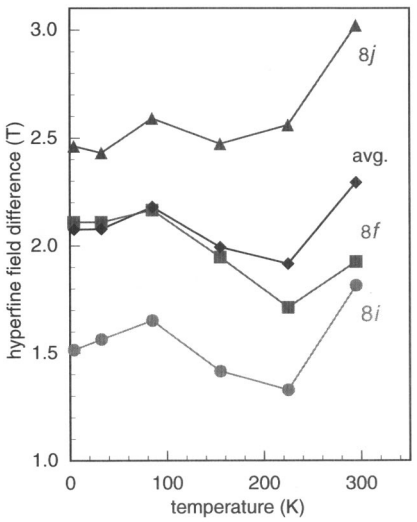

FIG. 6. The hyperfine field difference between $ErFe_{11}Ti$ and $ErFe_{11}TiH$ for the three iron sites and their average.

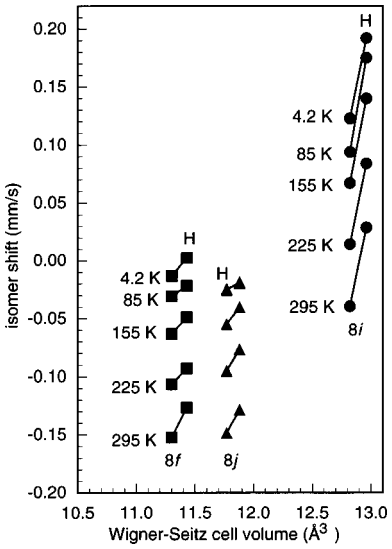

FIG. 8. The correlation between the isomer shift and the Wigner–Seitz cell volume of the three iron sites in $ErFe_{11}Ti$ and $ErFe_{11}TiH$.

B. Isomer shifts

The assignment and the temperature dependence of the three site average isomer shifts, and their weighted average, for $ErFe_{11}Ti$ and $ErFe_{11}TiH$ are shown in Figs. 7(a) and 7(b), respectively. The site average isomer shifts have been calculated from the δ_n values weighted with the percent contribution given by the binomial distribution. In agreement with the Wigner–Seitz cell analysis[38] of the three inequivalent iron sites, the sequence of isomer shifts, $8i > 8j > 8f$, follows the sequence of Wigner–Seitz cell volumes. Such a relationship between isomer shifts and Wigner–Seitz cell volumes has been observed in many R_2Fe_{17} compounds.[39,40] The overall increase in unit-cell volume accounts for the increase in the weighted average isomer shift upon hydrogenation. All of the 295 K isomer shifts are negative relative to α-iron as has been observed[43,44] in other iron–titanium compounds.

The temperature dependence of the weighted average isomer shifts shown in Fig. 7 has been fit[45,46] with the Debye model for the second-order Doppler shift. For both compounds, the resulting effective vibrating mass[46] is, as expected, 57 g/mol and the effective Mössbauer temperature is 360 ± 10 K. This temperature is typical of an intermetallic compound[31,40,47] and it would appear that the addition of the hydrogen has rather little influence on the Mössbauer temperature even though there is a one percent expansion of the lattice upon hydrogenation.

The relationship between isomer shifts and the Wigner–Seitz cell volumes is shown in Fig. 8. Upon hydrogenation, the Wigner–Seitz cell volumes[3,38] of the 8*f* and 8*i* sites increase, whereas that of the 8*j* site decreases slightly. The changes in the isomer shift correlate well with those in the Wigner–Seitz cell volumes because the 8*f* and 8*i* isomer shifts increase upon hydrogenation, whereas the 8*j* isomer shift decreases, see Figs. 7(a) and 7(b).

The changes in the isomer shift per titanium near neighbor are virtually independent of temperature at 0.04, -0.03, and -0.03 mm/s for $ErFe_{11}Ti$ and 0.05, 0.08, and

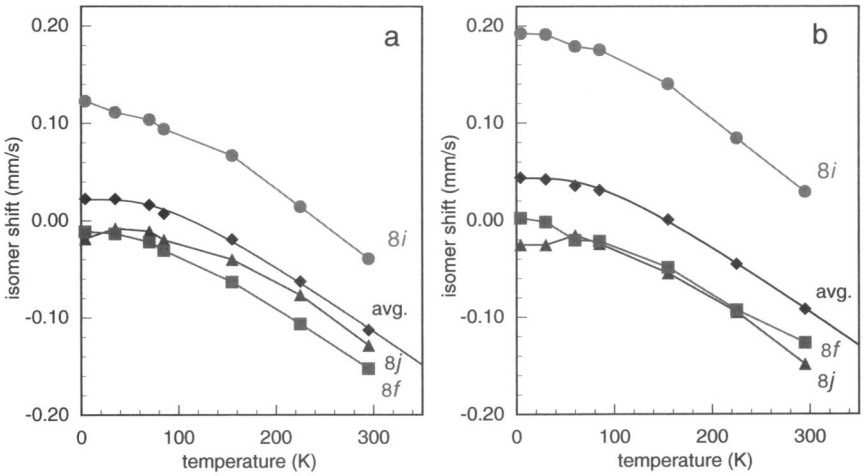

FIG. 7. The temperature dependence of the three site average isomer shifts and their average in $ErFe_{11}Ti$ (a) and $ErFe_{11}TiH$ (b).

-0.01 mm/s for $ErFe_{11}TiH$, for the 8*f*, 8*i*, and 8*j* sites, respectively. Such small changes have been observed[3,37] in $YFe_{11}Ti$ and $CeFe_{11}Ti$ and their hydrides. However, it seems difficult to rationalize the sign of these changes.

C. Quadrupole shifts

The observed quadrupole shifts in the Mössbauer spectra of $ErFe_{11}Ti$ and $ErFe_{11}TiH$ are small and lie between 0 and 0.2 mm/s and their changes upon hydrogenation are very small at between 0 and 0.1 mm/s. Small quadrupole shifts are expected because Mössbauer spectral studies[48] at 295 K of some related paramagnetic $RFe_{11}Ti$ and $RFe_{11}Mo$ compounds yield quadrupole splittings of at most 0.6 mm/s.

VI. CONCLUSIONS

From a macroscopic point of view, the insertion of hydrogen into $ErFe_{11}Ti$ to form $ErFe_{11}TiH$ expands the lattice by 1%, increases the Curie temperature by 56 K, increases the saturation magnetization by 1 μ_B per formula unit at both 5 and 300 K, and decreases the spin-reorientation temperature by ~ 10 K. From a microscopic point of view, the insertion of hydrogen increases all three iron hyperfine fields in agreement with the observed lattice expansion, increases the iron-57 isomer shifts of the 8*f* and 8*i* sites, and decreases the isomer shift of the 8*j* site, all changes that are in agreement with the changes in Wigner–Seitz cell volume upon hydrogen insertion. The presence of one titanium near neighbor in the environment of an iron site decreases the hyperfine field by ~ 2 T and changes the isomer shift by ~ 0.05 mm/s.

ACKNOWLEDGMENTS

The financial support of the University of Liège for Grant No. 2850006 is acknowledged with thanks. This work was partially supported by the U. S. National Science Foundation through Grant Nos. DMR95-21739 and INT-9815138, and the ''Centre National de la Recherche Scientifique, France'' through Grant Action Initiative No. 7418.

[1] K. H. J. Buschow, in *Electronic and Magnetic Properties of Metals and Ceramics, Materials Science and Technology*, Series, Vol. 3B, Part II, edited by K. H. J. Buschow (VCH, Berlin, 1994), p. 451.
[2] B. P. Hu, H. S. Li, J. P. Gavigan, and J. M. D. Coey, J. Phys.: Condens. Matter **1**, 755 (1989).
[3] G. J. Long, D. Hautot, F. Grandjean, O. Isnard, and S. Miraglia, J. Magn. Magn. Mater. **202**, 100 (1999).
[4] N. Plugaru, J. Rubin, J. Bartolomé, C. Piquer, and M. Artigas, Phys. Rev. B **65**, 134419 (2002).
[5] F. R. de Boer, Y. K. Huang, D. B. de Mooij, and K. H. J. Buschow, J. Less-Common Met. **135**, 199 (1987).
[6] D. B. de Mooij and K. H. J. Buschow, J. Less-Common Met. **136**, 207 (1988).
[7] K. H. J. Buschow, J. Magn. Magn. Mater. **100**, 79 (1991).
[8] L. Y. Zhang and W. E. Wallace, J. Less-Common Met. **149**, 371 (1989).
[9] O. Isnard, M. Guillot, S. Miraglia, and D. Fruchart, J. Appl. Phys. **79**, 5542 (1996).
[10] Bo Ping Hu, Ph. D. thesis, University of Dublin, Trinity College, 1990.
[11] K. H. J. Buschow, in Handbook of Magnetic Materials, edited by K. H. J. Buschow (Elsevier, Amsterdam, 1997), Vol. 10, p. 463.
[12] O. Isnard, S. Miraglia, M. Guillot, and D. Fruchart, J. Alloys Compd. **275**, 637 (1998).
[13] D. P. F. Hurley, Ph. D. thesis, Trinity College, Dublin, 1993.
[14] Q. Qi, Y. P. Li, and J. M. D. Coey, J. Phys.: Condens. Matter **4**, 8209 (1992).
[15] D. P. F. Hurley and J. M. D. Coey, J. Phys.: Condens. Matter **4**, 5573 (1992).
[16] A. V. Andreev, V. Sechovsky, N. V. Kudrevatykh, S. S. Sigaev, and E. N. Tarasov, J. Less-Common Met. **144**, L21 (1988).
[17] B. P. Hu, H. Sun, J. M. D. Coey, and J. P. Gavigan, Phys. Rev. B **41**, 2221 (1990).
[18] X. C. Kou, T. S. Zhao, R. Grössinger, H. R. Kirchmayer, X. Li, and F. R. de Boer, Phys. Rev. B **47**, 3231 (1993).
[19] L. Y. Zhang, E. B. Boltich, V. K. Sinha, and W. E. Wallace, IEEE Trans. Magn. **25**, 3303 (1989).
[20] K. Yu. Guslienko, X. C. Kou, and R. Grössinger, J. Magn. Magn. Mater. **150**, 383 (1995).
[21] O. Isnard and M. Guillot, J. Appl. Phys. **83**, 6730 (1998).
[22] S. A. Nikitin, I. S. Tereshina, V. N. Verbetsky, and A. A. Salamova, J. Alloys Compd. **316**, 46 (2001).
[23] I. S. Tereshina, S. A. Nikitin, V. N. Nikiforov, L. A. Ponomarenko, V. N. Verbetsky, A. A. Salamova, and K. P. Skokov, J. Alloys Compd. **345**, 16 (2002).
[24] A. Barlet, J. C. Genna, and P. Lethuillier, Cryogenics **31**, 801 (1991).
[25] C. Rillo, F. Lera, A. Badia, L. Angurel, J. Bartolomé, F. Palacio, R. Navarro, and A. J. Duyneveldt, in *Susceptibility of Superconductors and Other Spin Systems*, edited by R. A. Hein, J. L. Francavilla, and D. H. Liebenberg (Plenum, New York, 1992).
[26] E. Tomey, O. Isnard, A. Fagan, C. Desmoulins, S. Miraglia, J. L. Soubeyroux, and D. Fruchart, J. Alloys Compd. **191**, 223 (1993).
[27] A. Apostolov, R. Bezdushnyi, N. Stanev, R. Damianova, D. Fruchart, J. L. Soubeyroux, and O. Isnard, J. Alloys Compd. **265**, 1 (1998).
[28] O. Isnard, P. Vulliet, J. P. Sanchez, and D. Fruchart, J. Magn. Magn. Mater. **189**, 47 (1998).
[29] Z. W. Li, X. Z. Zhou, and A. H. Morrish, J. Phys.: Condens. Matter **5**, 3027 (1993).
[30] M. Brouha, K. H. J. Buschow, and A. R. Miedema, IEEE Trans. Magn. **10**, 182 (1974).
[31] F. Grandjean, O. Isnard, and G. J. Long, Phys. Rev. B **65**, 64429 (2002).
[32] Z. F. Gu, D. C. Zeng, Z. Y. Liu, S. Z. Liang, J. C. P. Klasse, E. Brück, F. R. de Boer, and K. H. J. Buschow, J. Alloys Compd. **321**, 40 (2001).
[33] G. J. Long, G. K. Marasinghe, S. Mishra, O. A. Pringle, Z. Hu, W. B. Yelon, D. P. Middleton, K. H. J. Buschow, and F. Grandjean, J. Appl. Phys. **76**, 5383 (1994).
[34] D. P. Middleton, S. R. Mishra, G. J. Long, O. A. Pringle, Z. Hu, W. B. Yelon, F. Grandjean, and K. H. J. Buschow, J. Appl. Phys. **78**, 5568 (1995).
[35] S. R. Mishra, G. J. Long, O. A. Pringle, D. P. Middleton, Z. Hu, W. B. Yelon, F. Grandjean, and K. H. J. Buschow, J. Appl. Phys. **79**, 3145 (1996).
[36] D. Hautot, G. J. Long, P. C. Ezekwenna, F. Grandjean, D. P. Middleton, and K. H. J. Buschow, J. Appl. Phys. **83**, 6736 (1998).
[37] I. S. Tereshina, P. Gaczynsku, V. S. Rusakov, H. Drulis, S. A. Nikitin, W. Suski, N. V. Tristan, and T. Palewski, J. Phys.: Condens. Matter **13**, 8161 (2001).
[38] L. Gelato, J. Appl. Crystallogr. **14**, 141 (1981).
[39] D. Hautot, G. J. Long, F. Grandjean, O. Isnard, and S. Miraglia, J. Appl. Phys. **86**, 2200 (1999).
[40] D. Hautot, G. J. Long, F. Grandjean, and O. Isnard, Phys. Rev. **62**, 11731 (2000).
[41] J. L. Dormann, Rev. Phys. Appl. **15**, 1113 (1980).
[42] F. Grandjean, P. C. Ezekwenna, G. J. Long, O. A. Pringle, P. L'Héritier, M. Ellouze, H. P. Luo, and W. B. Yelon, J. Appl. Phys. **84**, 1893 (1998).
[43] E. V. Mielczarek and W. P. Winfree, Phys. Rev. B **11**, 1026 (1975).
[44] J. Lu, H. J. Hesse, J. Zukrowski, J. Przewoznik, and G. Wortmann, in *Conference Proceedings, Vol. 50, International Conference of the Applications of the Mössbauer Effect*, edited by I. Ortalli (Italian Physical Society, Bologna, 1996), p. 243.
[45] G. J. Long, D. Hautot, F. Grandjean, D. T. Morelli, and G. P. Meisner, Phys. Rev. B **60**, 7410 (1999); *ibid.* **62**, 6829 (2000).
[46] R. H. Herber, in *Chemical Mössbauer Spectroscopy*, edited by R. H. Herber (Plenum, New York, 1984), p. 199.
[47] G. J. Long, O. Isnard, and F. Grandjean, J. Appl. Phys. **91**, 1423 (2002).
[48] F. Grandjean, R. P. Hermann, and G. J. Long (unpublished).